RSC Advances

This is an *Accepted Manuscript*, which has been through the Royal Society of Chemistry peer review process and has been accepted for publication.

Accepted Manuscripts are published online shortly after acceptance, before technical editing, formatting and proof reading. Using this free service, authors can make their results available to the community, in citable form, before we publish the edited article. This *Accepted Manuscript* will be replaced by the edited, formatted and paginated article as soon as this is available.

You can find more information about *Accepted Manuscripts* in the Information for Authors.

Please note that technical editing may introduce minor changes to the text and/or graphics, which may alter content. The journal's standard Terms & Conditions and the Ethical guidelines still apply. In no event shall the Royal Society of Chemistry be held responsible for any errors or omissions in this *Accepted Manuscript* or any consequences arising from the use of any information it contains.

ROYAL SOCIETY OF CHEMISTRY

www.rsc.org/advances

Please do not adjust margins

Journal Name

ARTICLE

Synthesis, mophology and spectroscopic properties of red-luminescent rhombohedral YOF: Yb^{3+}, Er^{3+} powders

Received 00th January 20xx,
Accepted 00th January 20xx

DOI: 10.1039/x0xx00000x

www.rsc.org/

Lizhen Sun[a, b], Jianfu Pan[a, b], Xiaobin Zhang[a, b], Heng Wang[c], Lingyun Li[* a, b] and Yan Yu[* a, b]

YOF: Yb^{3+}, Er^{3+} powders with rhombohedral phase were successfully synthesized by using a modified Sol-Gel method with calcinating under a temperature range between 400 °C and 600 °C. A systematic study on the temperature-dependent morphology and spectroscopic properties of rhombohedral YOF: Yb^{3+}, Er^{3+} powders have been performed. The YOF: Yb^{3+}, Er^{3+} powders that prepared at 400 °C and 500 °C exhibit a plate growth habit, while the powder that prepared at 600 °C shows a sintering property. When excited by 980 nm laser beam, all of the rhombohedral YOF: Yb^{3+}, Er^{3+} powders show efficient red light emission with light wavelength ranging from 630 nm to 700 nm. The upconversion mechanism and luminescence decay properties were discussed in detail.

Introduction

Upconversion lanthanide ion doped oxyfluorides, REOF (RE=La, Y, Gd, Lu), have been taken under extensive investigation owing to potential applications in lighting and displaying fields, bio-sensing, enhancing solar cell efficiency etc.[1-4] Most of the topic of interest is a combination of good chemical durability and excellent mechanical strength of oxides with superior luminescence quantum efficiency associated to fluorides, for which the probability of non-radiative transitions of excited Ln^{3+} ion by matrix is rather low.[5-7] Er^{3+}, Yb^{3+} co-doped YOF (YOF: Yb^{3+}, Er^{3+}) is well known as an important member of lanthanide ion doped REOF series of upconversion materials. It can be obtained with highly efficient upconversion luminescence (UCL), which is characteristic of low phonon energy of around 400 cm^{-1} owing to the reduced multi-phonon relaxation rates in it.[8] In the past few years, many efforts have been made to find a pure and single-phased stoichiometric YOF, which is generally presented in rhombohedal, tetragonal, or cubic phase. And it has been known that phase tansition among the above phases may be obtained by controlling the reaction temperature.[9-11]

Up to now, many groups have concentrated their efforts on the determination of new synthetic routes and characterization of lanthanide ion doped YOF. For example, Dutton et al. reported a solid-state synthetic route employing polytetra fluoroethylene and the rare-earth oxides, for the purpose of YOF preparation, which need a post formation annealing and a second firing process with a temperature higher than 800 °C.[12] Rakov and Maciel prepared Er^{3+} and Tm^{3+} co-doped YOF powders with spectrally pure red color emission by combustion synthesis combined with a heat treatment procedure at 750 °C for 2h. The results showed that the energy transfer (ET) process between Er^{3+} and Tm^{3+} ions in YOF was much more efficient than that observed in Y_2O_3 powder.[13] Similar phenomena have also been observed in other researches.[14-16] In the work reported by Wen et al., pure vernier phase YOF with orthorhombic symmetry was prepared via a room-temperature co-precipitation of Y^{3+} ions with CO_3^{2-} and F^- in water and a subsequent thermal decomposition at 400 °C.[17] Li et al. have performed a detailed study of the influence of pH values, fluoride sources and reaction time on the sizes and morphologies of Ln^{3+} doped YOF nano-/microcrystals synthesized via a urea based homogeneous precipitation method followed by a heat-treatment process at 550 °C in air for 3h.[18] However, the approaches reported above suffer from drawbacks such as rigorous conditions, time consuming and complicated technical processes, some even require expensive chemicals and equipments, which severely restrict their technological applications.[19] The Sol-Gel method, on the other hand, is a wet chemical technique with low cost and high yield employed in producing single- or multi-phase oxyfluoride powders. Based on the Sol-Gel Pechini method, Grzyb and co-workers have successfully prepared a series of LnOF: Eu^{3+} (Ln=La, Gd, Y) nanocrystals with annealing at the temperature range of 500-900 °C. Rare earth nitrates and ammonium fluorides were used as resources for Ln and F, while citric acid was used as complexing agent for cations. The authors have also investigated the optimal annealing conditions to obtain single-phase (tetragonal or rhombohedral) structure and the optimum Eu^{3+} concentration to obtain the best luminescence efficiency for each phase. However, in the work, the rhombohedral YOF was obtained

[a] Key Laboratory of Eco-materials Advanced Technology (Fuzhou University), Fujian Province University.
[b] College of Materials Science and Engineering, Fuzhou University, New Campus, Minhou, Fujian Province 350108, China. Email: lilingyun@fzu.edu.cn, yuyan@fzu.edu.cn
[c] College of Science, Guilin University of Technology, Guilin 541008, PR China

RSC Advances Accepted Manuscript

Please do not adjust margins

only when the heat-treatment temperature was raised above 700 °C.[20-22] Therefore, there is still need to find a convenient method to synthesize YOF: Yb^{3+}, Er^{3+} with moderate reaction conditions and heat treatment under relative lower temperature. In addition to this, the rhombohedral YOF have aroused much more interests than other phases because of their fascinating structural characteristics.

This paper reports a facile sol-gel method with relatively lower calcinating temperature (400 °C) to prepare spectrally pure rhombohedral YOF: Yb^{3+}, Er^{3+} powders with efficient red emission under a 980 nm laser excitation. Meanwhile, the growth mechanism and spectroscopy properties have been investigated.

Experimental

Materials and methods

The rare earth oxides Re_2O_3 (Re=Y, Yb, Er) (99.99%) were purchased from Sinopharm Chenmical Reagent Co. China. The rare-earth nitrate solid powders, $Y(NO_3)_3$, $Yb(NO_3)_3$, and $Er(NO_3)_3$ were prepared by dissolving the corresponding metal oxide in nitric acid at 80 °C with agitation, and then evaporate the excess solvents. Trifluoroacetic acid (TFA) obtained from Aladdin was used as the fluoride source. Isopropanol, ethanol, and deionized water were used as solvents. All of the reagents were used as received without further purification.

In a typical synthesis, 1 mmol of rare-earth nitrate (0.03 mmol of $Er(NO_3)_3{\cdot}5H_2O$, 0.17 mmol of $Yb(NO_3)_3{\cdot}5H_2O$, 0.8 mmol of $Y(NO_3)_3{\cdot}6H_2O$) powders were mixed with 4 ml of isopropanol, 4 ml of ethanol and 1ml of deionized water. 1 ml of TFA was slowly dropped into the solution under vigorous stirring. Afterwards, the mixed solution was kept under constant stirring at a room temperature for 3 h to obtain a transparent sol. Then, the as-prepared sol was transferred into an alumina crucible, and dried at 100 °C in order to evaporate the excess free water. After drying for 3h, a monolithic gel would be obtained. The gel obtained above was then used as precursor and calcinated under certain temperature for 1 h in a resistance furnace. The heating rate is 4 °C/min. When the calcinating procedure completed, the furnace was then allowed to cool to room temperature naturally and the YOF: Yb^{3+}, Er^{3+} powders were collected by grinding. For the purpose of comparison, the calcinating temperature was set from 350 °C to 800 °C for different samples.

Characterization

X-ray diffraction (XRD) data of the obtained powder samples was collected by using a Miniflex II type X-ray diffractometer operating with Cu Kα1 radiation and a graphite diffracted beam monochromator. XPS measurement was performed on a ESCALAB 250 type instrument from Thermo Scientific. The TGA and DSC curves were measured on STA449C from NETZSCH.

Scanning electron microscopy (SEM) images were measured on a JSM6700F SEM (Zeiss). Samples used for SEM analysis were coated with Carbon. TEM and HRTEM images were recorded on TECNAI G2F20 from FEI. Upconversion emission spectra of the as prepared YOF: Yb^{3+}, Er^{3+} powders were collected using a 980 nm laser excitation by a continuous-wave laser diode. UCL decay curves were measured with a customized ultraviolet (UV) to mid-infrared steady-state laser and a phosphorescence lifetime spectrometer (FSP920-C, Edinburgh) equipped with a digital oscilloscope (TDS3052B, Tektronix) and a tunable mid-band Optical Parametric Oscillator (OPO) pulse laser as the excitation source (410–2400 nm, 10 Hz, pulse width of 5ns, Vibrant 355II, OPOTEK). All the measurements were performed at room temperature.

Results and discussion

Phase identification

Fig. 1 shows the XRD patterns of the samples calcinated at different temperatures. The pattern of the sample annealed at 350 °C can be identified with two phases: tetragonal and rhombohedral YOF phases. However, during the temperature range of 400-600 °C, all the peaks of each sample are characteristic ones of rhombohedral YOF phase, which are in good agreement with the standard card with JCPDS No. 071-2100. No impurity peaks can be observed, revealing that tetragonal YOF phase has transformed completely into the rhombohedral phase with high crystallinity. Furthermore, samples obtained by calcinating above 600 °C were mixtures of YOF and Y_2O_3, which was a final product of oxyfluorides thermal decomposition. Because other parameters are basically identical, the difference of the phase composition is probably related to the the calcinating temperature.

In order to determine the phase purity of the calcinated products, the compositions of the samples that calcianted at 400 °C, 500 °C and 600 °C (YOF:Yb^{3+}, Er^{3+}@400 °C, YOF:Yb^{3+}, Er^{3+}@500 °C and YOF:Yb^{3+}, Er^{3+}@600 °C) were fitted by Rietveld method through GSAS software.[23] Both rhombohedral YOF (71-2100) and tetragonal YOF (06-0347) were used as initial structure model for fitting of YOF:Yb^{3+}, Er^{3+}@400 °C and 500 °C samples. Meanwhile, for YOF:Yb^{3+}, Er^{3+}@600 °C, cubic Y_2O_3:Yb^{3+},Er^{3+} was applied as the second phase, i.e. the strating models for the structure refinement of YOF:Yb^{3+}, Er^{3+}@600 °C sample are rhombohedral YOF (71-2100) and cubic Y_2O_3 (41-1105). Results of Rietveld refinement shows that it is hard to find impurity phase in YOF:Yb^{3+}, Er^{3+}@400 °C, 500 °C and 600 °C samples. The XRD pattern difference between YOF:Yb^{3+}, Er^{3+}@400 °C， 500 °C and 600 °C samples is mainly caused by the difference between their lattice constants.

Element analysis

The XPS spectra of YOF:Yb^{3+}, Er^{3+}@400 °C， 500 °C and 600 °C samples were also measured. The XPS survey spectra of the

RSC Advances Accepted Manuscript

This journal is © The Royal Society of Chemistry 20xx

YOF:Yb^{3+}, Er^{3+} samples calcinated 400 °C， 500 °C and 600 °C are almost the same, as shown in Fig. 2. Besides peaks of Y, Yb, Er, O and F which come from the calcinated products, C_{1S} peak that caused by surface contamination of samples is also observed. Fig. 3 shows the XPS speatra of Yb_{3d}, Y_{3d} and Er_{3d} core levels of YOF:Yb^{3+}, Er^{3+}@400 °C， 500 °C and 600 °C samples. Since the doping amount of Yb and Er is small in these samples, the peak intensity that corresponding to Yb or Er is relative weak than that corresponding to element Y. Meanwhile, bands of Yb_{3d}, Y_{3d} exhibit clear splitting property because of the spin–orbit coupling of 3*d* electron. However, the splitting of Er_{3d} band is not obvious. In order to investigate the influence of calcinating temperature on chemical bonding state of Y ion, the XPS spectra of Y_{3d} core levels were recorded and are shown in Fig. 4. As revealed by this figure, the shape of Y_{3d} band of YOF:Yb^{3+}, Er^{3+} samples that calcinated 400 °C， 500 °C and 600 °C are identical to each other. All of the spectra shown in Fig. 4 could be deconvoluted into two bands with peaks at 157.0 eV and 159.1 eV corresponding to Y that bonding with anions. The peaks energies of Y_{3d} XPS spectrum of YOF:Yb^{3+}, Er^{3+} sample show no shift when the calciniating temperature elevates from 400 °C to 600 °C. Since the binding energy of Y_{3d} is sensitive to the change of bonding circumstance, results that derived from Fig. 4 demonstrate that the chemical composition YOF:Yb^{3+}, Er^{3+}@400 °C， 500 °C and 600 °C samples are same and there is only one kind of Y ion in these samples.

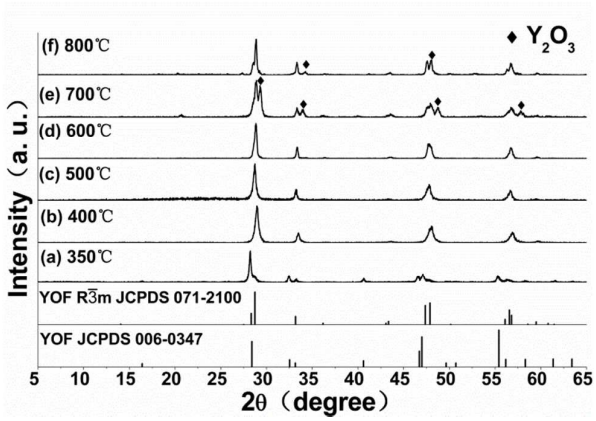

Fig. 1 XRD patterns of the as-prepared YOF: Yb^{3+}, Er^{3+} powders annealed at different temperatures for 1 h in air compared with standard data of tetragonal YOF (JCPDS 006-0347) and rhombohedral YOF (JCPDS 071-2100) as a reference: (a) 350 °C, (b) 400 °C, (c) 500 °C, (d) 600 °C, (e) 700 °C, (f) 800 °C.

The quantitative analysis of elements based on XPS spectra reveals that there are F deficiencies in all of YOF:Yb^{3+}, Er^{3+}@400 °C， 500 °C and 600 °C samples (F/(Y+Yb+Er) <1, O/(Y+Yb+Er)=1). This might be caused by the ambient calcinating atmosphere which does not contain fluoride element. Meanwhile, the quantitative analysis of Y, Yb and Er

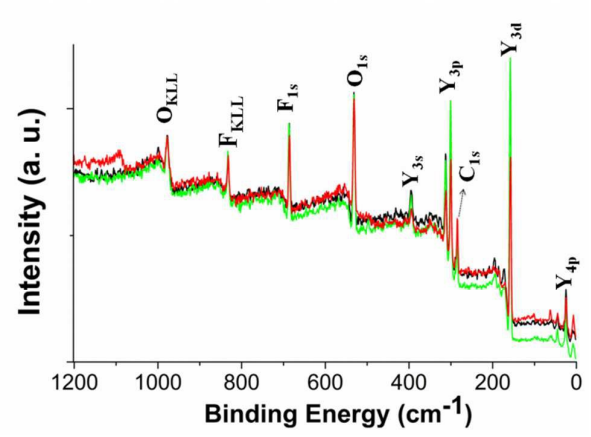

Fig. 2 The XPS survey spectra for the YOF:Yb^{3+}, Er^{3+}samples calcinated at 400 °C (Black line)， 500 °C (Green line) and 600 °C (Red line).

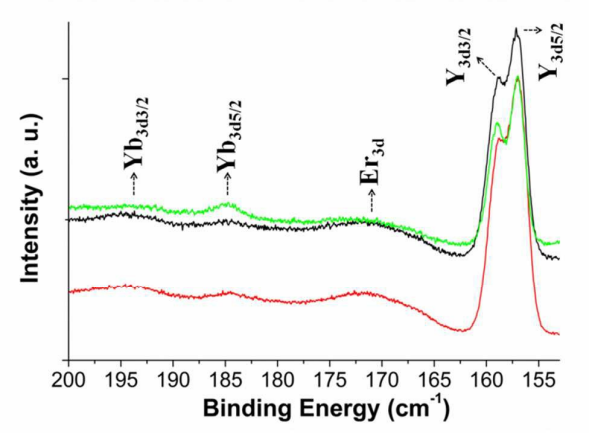

Fig. 3 The XPS spectra of Yb_{3d}, Y_{3d} and Er_{3d} core level of YOF:Yb^{3+}, Er^{3+} samples calcinated at 400 °C (Black line)， 500 °C (Green line) and 600 °C (Red line) samples.

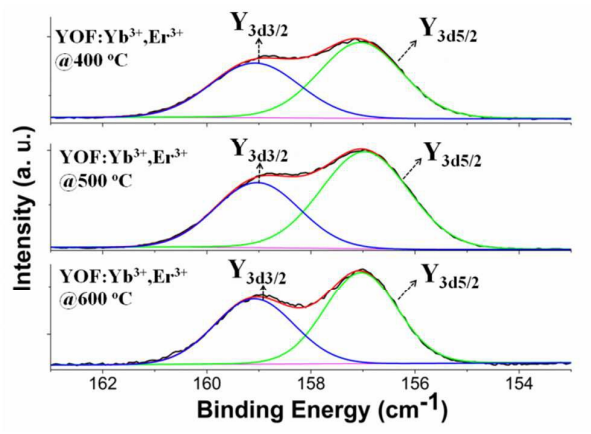

Fig. 4 The XPS spectra of Y_{3d} core level for YOF:Yb^{3+}, Er^{3+} samples calcinated at 400 °C, 500 °C and 600 °C samples.

RSC Advances Accepted Manuscript

shows that the ratios of Yb/Y and Er/Y are close to 0.17/0.8 and 0.03/0.8 (setting ratios in raw materials).

The elemental composition of the YOF:Yb^{3+}, Er^{3+}@400 °C, 500 °C and 600 °C samples were also measured by means of ICP-AES. The ratio between Y, Yb and Er elements derived from the result of ICP-AES is listed in Tab. 1. One can find that the ratios between Y, Yb and Er elements are not consistent with those derived from XPS analysis, for example, the ratios of Yb/Y and Er/Y of YOF:Yb^{3+}, Er^{3+}@400 °C listed in Tab. 1 is 0.147/0.8 and 0.028/0.8, which are both less than the setting ratios in raw materials.

Tab. 1 Relative contents (mol.%) of Y, Yb and Er elements measured by ICP-AES.

Samples	Y	Yb	Er
YOF:Yb^{3+}, Er^{3+}@400 °C	82.1	15.1	2.8
YOF:Yb^{3+}, Er^{3+}@500 °C	82.2	14.0	2.8
YOF:Yb^{3+}, Er^{3+}@600 °C	81.5	15.8	2.7

Since ICP-AES measurement result reveals the volume phase distribution of the measured elements, the difference on relative contents of Y, Yb and Er elements derived from ICP-AES and XPS spectra demonstrates that segregation coefficients of Yb and Er are less than 1 in rhombohedral YOF. That's to say, the distribution of Yb and Er ions in YOF is inhomogenous.[24,25]

Summarizing the results obtained by Rietveld structure refinement and XPS analysis, it could be concluded that samples calcinated at 400 °C, 500 °C and 600 °C are rhombohedral YOF:Yb^{3+}, Er^{3+}. Therefore, the YOF:Yb^{3+}, Er^{3+}@400 °C, 500 °C and 600 °C samples with rhombohedral symmetry, prepared at the temperature range of 400–600 °C, were taken for further investigation.

Morphology properties

The SEM images of the as-prepared YOF: Yb^{3+}, Er^{3+} samples are illustrated in Fig. 5-7. From low magnification SEM images given in Fig. 5(a) and Fig. 6(a), one can see that both of the YOF: Yb^{3+}, Er^{3+}@ 400 °C and YOF: Yb^{3+}, Er^{3+}@ 500 °C are composed of irregular micro-plate clusters with some particles aggregating among them. Furthermore, the SEM images with higher magnification (Fig. 5(b) and Fig. 6(b)) reveal that there are many tiny pores on the surface of the irregular plates, which is caused by the evaporation of organic matter during the calcinating procedure of gel. Meanwhile, the surface of the plates of YOF: Yb^{3+}, Er^{3+}@ 400 °C and YOF: Yb^{3+}, Er^{3+}@ 500 °C observed in SEM images is not smooth. In fact, the plates with irregular morphology in Fig. 5 and Fig. 6 are crystals of rhombohedra YOF. Nevertheless, the morphology of the YOF: Yb^{3+}, Er^{3+}@ 600 °C product varies remarkably from the others. As shown in Fig. 7(a), the calcinating products of YOF: Yb^{3+}, Er^{3+}@ 600 °C are composed of a lot of interconnected sub-micro spheres with an average size of about 400 nm, forming a highly porous morphology. This character of samples prepared by Sol-Gel method is presumably due to the sintering of gel precursors. Meanwhile, many plates with standard hexagonal shape were found standing on the surface of the porous product. The thickness of the hexagonal plates is about 20 nm. It can be concluded that the calcinating temperature has obvious effects on the morphologies of the final products. Concretely speaking, when heated at the lower temperature stage (400°C and 500 °C), the gel precursors gradually transformed into plated shape crystals with the volatilization of organic solvents, resulting in the formation of plentiful aggregates combined with tiny pores on the surface. However, once the temperature was increased to 600 °C, the plated shape crystals were sintered into interconnected spherical grains to form a porous morphology, and the crystallinity of the grains would be higher than the plates that constitute products of YOF: Yb^{3+}, Er^{3+} @ 400 °C and YOF: Yb^{3+}, Er^{3+} @ 500 °C. Moreover, regular and monodispersed hexagonal plates standing at the surface of the porous YOF: Yb^{3+}, Er^{3+} @ 600 °C can be also observed in the SEM images (Fig. 7(a)). Different from the crystals that constitute YOF: Yb^{3+}, Er^{3+} @ 400 °C or YOF: Yb^{3+}, Er^{3+} @ 500 °C products, the plates shown in Fig. 7(a) have perfectly hexagonal shape with flat top/bottom surfaces as well as regular edges. Further careful examination of a typical hexagonal plate shows that the surfaces of these plates are smooth without any cracks or pores. It's known that the shape of single crystal is determined by the symmetry of unit cell and the anisotropic growth rate.[26, 27] Meanwhile, as revealed by the analysis of XRD patterns, the doping of Er^{3+} and Yb^{3+} does not change the crystal symmetry of YOF: Yb^{3+}, Er^{3+} @ 600 °C product, then the effect of Er^{3+} and Yb^{3+} doping on the shape of rhombohedral YOF single crystal could be negelected. Fig. 8 schematically illustrates the structure and coordination environments of rhombohedral YOF with $R\bar{3}m$ space group. The structure of the stoichiometric YOF can be derived from the fluoride CaF_2 cubic cell with a small distortion. As shown in Fig. 8, the Y atom occupies a site with C_3 point symmetry resulting from an eight-fold coordination to four O atoms and four F atoms across the fixed sites to form the ordered layers.[28] Besides, the Y^{3+} cation frameworks can be viewed as a bicapped trigonal antiprism with the cubes sharing edges to form a 3D crystal network of polyhedral, wherein all ions (F^-, O^{2-}, and Y^{3+}) occupy the six-fold 6c Wyckoff positions.[29,30] Based on the structure properties discussed above, the shape of rhombohedral YOF could be predicted and the result is shown in Fig. 7(b). One can see that the (001) faces are well developed and the $(L0\bar{L})$, $(L0\bar{L})$, $(0L\bar{L})$, $(0LL)$, $(L\bar{L}\bar{L})$, $(\bar{L}L\bar{L})$ (L=1 or $\bar{1}$) faces are also appeared. The shape of hexagonal plates shown in Fig. 7(a) is in good agreement with the predicted shape of single crystal of YOF with space group of $R\bar{3}m$.

RSC Advances Accepted Manuscript

This journal is © The Royal Society of Chemistry 20xx

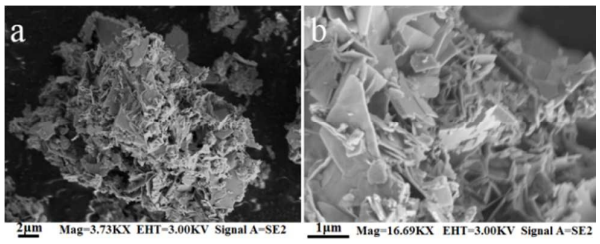

Fig. 5 SEM images of YOF: Yb^{3+}, Er^{3+}@ 400 °C: (a) 3.73 KX, (b) 16.69 KX.

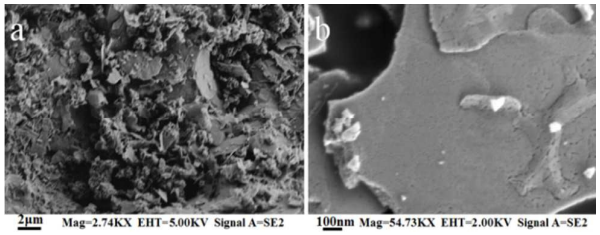

Fig. 6 SEM images of YOF: Yb^{3+}, Er^{3+}@ 500 °C: (a) 2.74 KX, (b) 54.73 KX.

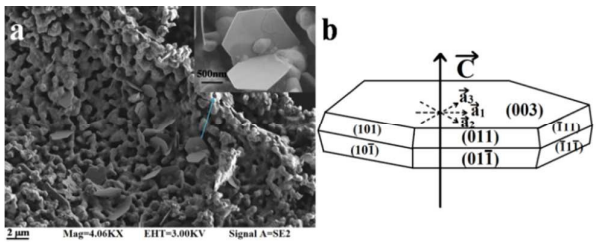

Fig. 7 SEM image of YOF: Yb^{3+}, Er^{3+} @ 600 °C (a) and the predicted shape of rhombohedral YOF (b).

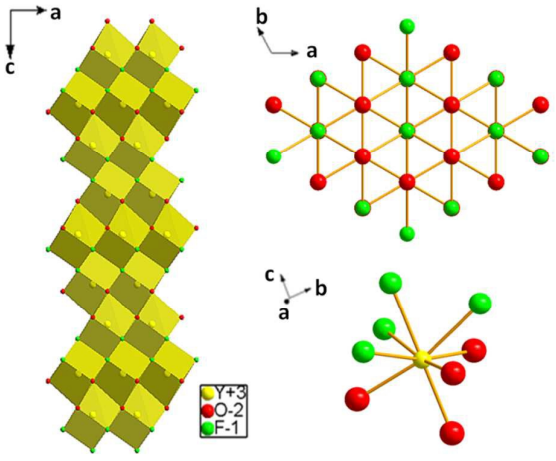

Fig. 8 Structure properties of the rhombohedral phase YOF.

TEM and HRTEM images of YOF:Yb^{3+}, Er^{3+}@400 °C, 500 °C and 600 °C samples were measured to get more structure information (Fig. 9). The TEM images of YOF:Yb^{3+}, Er^{3+}@400 °C and 500 °C (a, c) show that the samples calcinated at 400 °C and 500 °C have plate structures, which is in line with SEM images. Besides light gray part in the TEM image of YOF:Yb^{3+}, Er^{3+}@600 °C (e), there is a little dark part coexisting at the lower right corner of this image, showing that the thickness of YOF:Yb^{3+}, Er^{3+}@600 °C is inhomogeneous. Fig. 9 (b) and (d) show the HRTEM images of YOF:Yb^{3+}, Er^{3+}@400 °C and YOF:Yb^{3+}, Er^{3+}@500 °C, respectively. The inter-planar distance between the adjacent lattice fringes is determined to be 0.270 nm that corresponds to the (104) plane of the rhombohedral YOF. The HRTEM image of YOF:Yb^{3+}, Er^{3+}@600 °C sample is shown in Fig. 9 (f), the inter-planar distance between the adjacent lattice fringes is determined to be 0.3105 nm, which is in line with the inter-planar spacing of (012) plane of the rhombohedral YOF.

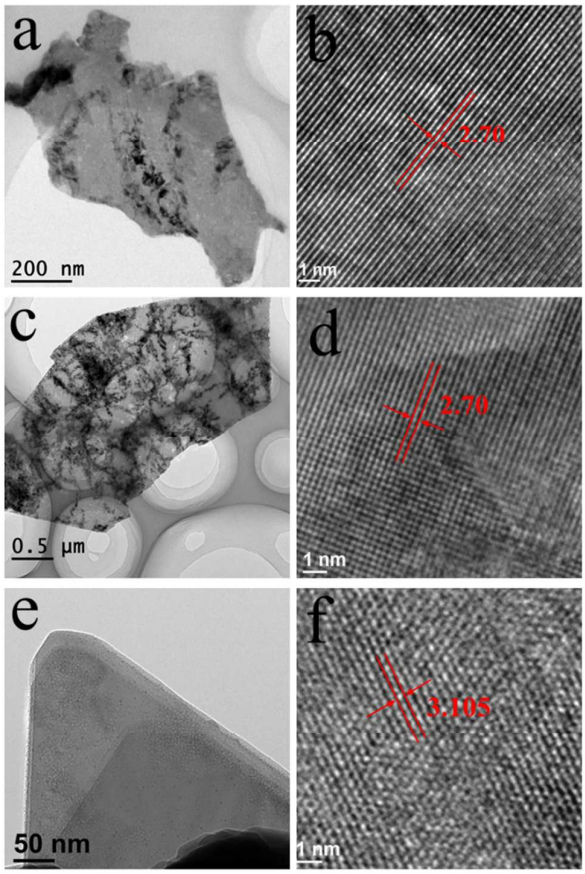

Fig. 9 TEM and HRTEM images of YOF:Yb^{3+}, Er^{3+}@400 °C (a, b), YOF:Yb^{3+}, Er^{3+}@500 °C (c, d) and YOF:Yb^{3+}, Er^{3+}@600 °C (e, f), the unit of lattice fringes distance is Angstrom.

Thermal properties

TGA and DSC curves of the gel precursor were recorded from room temperature to 890 °C, and the result is shown in Fig. 10. There are three weight loss stages during the heating procedure of precursor. The first slow weight loss occurs in temperature range from 100 °C to 200 °C, which corresponds to the loss of occlusion water, ehanol and isopropanol absorbing on the sample. The second mass loss occurring between 200 °C and 350 °C is probably attributed to the loss of

RSC Advances Accepted Manuscript

crystal water and the decomposition of a small amount of trifluoroacetate, and the third abrupt descent of the TGA pattern between 320 °C and 380 °C should be caused by further decomposition of trifluoroacetate and the formation of YOF. The intense endothermic peak with center at 368 °C appeared on the DSC curve indicates that formation of tetragonal YOF and transition of rhombohedral YOF from tetragonal phase complete before 400 °C, which is in line with the XRD pattern result. However, there is no evident weight loss or sharp endothermic peak appearing on the TGA or DSC curve as the temperature increased above 600 °C, i.e. the transition between YOF:Yb^{3+}, Er^{3+} and Y_2O_3:Yb^{3+}, Er^{3+} might be a gradual process caused by gradual substitution of oxygen atom for fluoride atom. This phenomenon is in accordance with the result of XRD pattern. Analysis of the temperature dependent XRD patterns of the calcinated products reveals that Y_2O_3:Yb^{3+}, Er^{3+} appears when the gel precursor is calcinated at temperature beyond 600 °C. However, even when the gel precursor calcinated at 800 °C, there is still YOF:Yb^{3+}, Er^{3+} existing in the obtained product with weight fraction decreasing, which means that phase transition of YOF:Yb^{3+}, Er^{3+} to Y_2O_3:Yb^{3+}, Er^{3+} is a slow procedure.

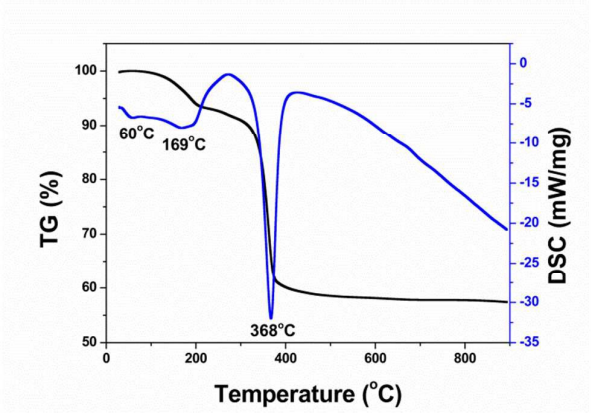

Fig. 10 TGA and DSC curves of the as-prepared precursor.

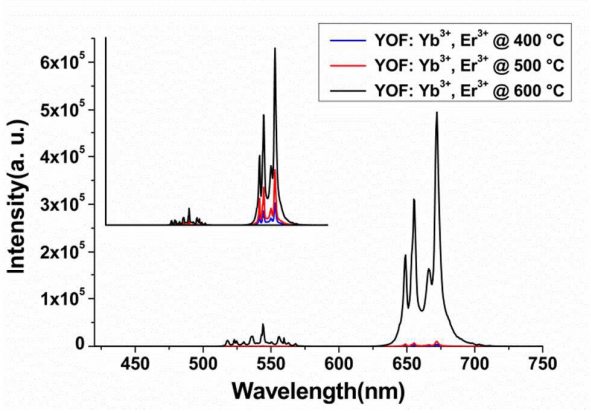

Fig. 11 UCL spectra of the as-prepared YOF: Yb^{3+}, Er^{3+} samples annealed at different temperatures.

Upconversion luminescence properties

In order to further investigate the dependence of the luminescence intensity on the morphologies, the UCL spectra of the as-synthesized YOF: Yb^{3+}, Er^{3+} samples have been measured and shown in Fig. 11. The red emission originating from $^4F_{9/2}\rightarrow{}^4I_{15/2}$ transition of Er^{3+} (λ_{peak}=672 nm) can be observed as a dominant one with much higher intensity compared to the green emission centered at 593 nm, which can be assigned to $^2H_{11/2}$, $^4S_{3/2}\rightarrow{}^4I_{15/2}$ transitions. The change of the emisssion intensity is not obvious when the temperature increases from 400 °C to 500 °C, which can be explained by the similar morphologies and crystallinity of the YOF: Yb^{3+}, Er^{3+} @ 400 °C and YOF: Yb^{3+}, Er^{3+} @ 500 °C products. As expected, the emission of $^4F_{9/2}\rightarrow{}^4I_{15/2}$ transition of YOF: Yb^{3+}, Er^{3+} @ 600 °C increases drastically and the intensity is about 146 times higher than that of the YOF: Yb^{3+}, Er^{3+} @ 400 °C. The reason for this observation is probably related to the enhancement of crystallinity of YOF: Yb^{3+}, Er^{3+} @ 600 °C. In order to research the evolution of the UCL spectrum, the intensity of the YOF: Yb^{3+}, Er^{3+} @ 600 °C was reduced by 15 times and compared with spectra of YOF: Yb^{3+}, Er^{3+} @ 400 °C and YOF: Yb^{3+}, Er^{3+} @ 500 °C, as shown in the inset of Fig. 11. It can be seen clearly that all three samples share a similar pattern without any shift of the emission peaks except from the intensity. This phenomenon demonstrates that the Er^{3+} ions occupy lattice sites with the same crystal field circumstance in all of the YOF: Yb^{3+}, Er^{3+} @ 400 °C, 500 °C and 600 °C products, i.e., the phase of all products are identical, which is confirmed by the XRD patterns.

The stark levels splitting of excited states of Er^{3+} in YOF:Yb^{3+}, Er^{3+}@400 °C， 500 °C and 600 °C samples is obvious in the UCL spectra. This property of the as obtained rhombohedral YOF:Yb^{3+}, Er^{3+} samples in our work is in accordance with that reported by T. Passuello and Y. Zhang et.al, who pointed out that the clear splitting of stark levels of Er^{3+} ions indicates that environment around the rare earth ions is quite ordered.[31,32]

Luminescent decay curves of $^2H_{11/2}\rightarrow{}^4I_{15/2}$ and $^4F_{9/2}\rightarrow{}^4I_{15/2}$ transition of Er^{3+} in different samples are recorded by monitoring the emissions at 536 nm and 672 nm, respectively. As shown in Fig. 12, all of the decay curves feature non-single-exponential characterization, which could be fitted well by a second exponential decay function with formula $y=A_0\exp(-x/\tau_1)+B_0\exp(-x/\tau_2)$, where τ_1 and τ_2 represent the luminescent lifetime of different centres in the crystal. The fitting results of the decay curves are shown in Tab. 2, from which we can see that both of the curves originating from decay of $^2H_{11/2}$ and $^4F_{9/2}$ levels for every sample could be divided into two parts, i.e. a fast decay part and a slow one. Generally, the non-single-exponential character of the luminescent decay curves in a luminescent material might be caused by the fact that there are more than one kind of active centres in the material or that there is energy transfer between different active centres. However, the XRD patterns of the samples reveal that the phase constitution of the products, which were calcinated between 400 °C and 600 °C, is pure rhombohedral YOF: Yb^{3+},Er^{3+}. Indeed, there is only one kind of lattice site in

RSC Advances Accepted Manuscript

This journal is © The Royal Society of Chemistry 20xx

rhombohedral YOF structure that could be occupied by the Er^{3+} and Yb^{3+} ions. In fact, a dual nature of the morphology of YOF: Yb^{3+}, Er^{3+} @ 400 °C, 500 °C and 600 °C could be found by a close observation on the SEM images, as shown in Fig. 5-7. For instance, besides the plates as dominant products of YOF: Yb^{3+}, Er^{3+} @ 400 °C, there are also many particles aggregating to disperse between the plates. Similar phenomenon could be found in YOF: Yb^{3+}, Er^{3+} @ 500 °C product. Furthermore, the morphology duality is more obvious in YOF: Yb^{3+}, Er^{3+} @ 600 °C, which has been discussed above. It's known that the luminescent decay character of materials in nano- or micrometer is sensitive to the morphology.[33-36] Although the products of the YOF: Yb^{3+}, Er^{3+} @ 400 °C, 500 °C and 600 °C are identical to pure rhombohedral phase, the morphology duality makes the luminescence decay of the products deviate from single-exponential property. On the other hand, the lifetime of YOF: Yb^{3+}, Er^{3+} @ 400 °C and YOF: Yb^{3+}, Er^{3+} @ 500 °C is reasonably expected to be similar within the scope of instrument error, while that of YOF: Yb^{3+}, Er^{3+} @ 600 °C is characteristic of a remarkable rising as the temperature increases, indicating the reduction of non-radiative transition procedure.[37, 38] This phenomenon could be also interpreted by the enhancement of crystallinity of YOF: Yb^{3+}, Er^{3+} samples produced by higher calcinating temperature, which is consistent with the results of SEM and UCL spectra analyses.

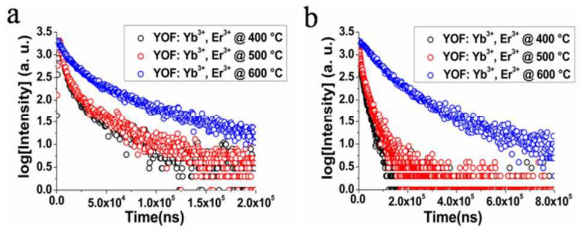

Fig. 12 UCL decay curves from $^2H_{11/2}$→$^4I_{15/2}$ (a) and $^4F_{9/2}$→$^4I_{15/2}$ (b) of Er^{3+} in different samples, monitoring the Er^{3+} emissions at 536nm and 672nm, respectively.

Tab. 2 Summary of the decay lifetime of $4S_{3/2}$ and $4F_{9/2}$ excited states and the corresponding compositions of the samples with different calcinating temperatures.

Samples	Decay lifetime (μs)				Composition
	4F9/2 (672m)		2H11/2 (536 nm)		
	Slow	fast	Slow	fast	
YOF: Yb^{3+}, Er^{3+} @ 400 °C	19.5	4.4	19.3	2.8	plates, particles
YOF: Yb^{3+}, Er^{3+} @ 500 °C	23.0	4.3	18.3	2.6	plates, particles
YOF: Yb^{3+}, Er^{3+} @ 600 °C	225.3	61.5	46.84	9.0	porous bulk, nanometer singlecrystal

In order to determine the number of photons involved in the up-conversion emission process of rhombohedral YOF: Yb^{3+}, Er^{3+} samples, the green and red luminescence intensities (I_{em}) are recorded as a function of the 980 nm excitation intensity density (I_{IR}). Since the relation of I_{IR} and I_{em} could be described as

$$I_{IR} : I_{em} \propto I_{IR}^{n},$$

where the number of absorbed photons per visible phonon emitted, *n*, is identical to the slope of fitted line of the double logarithmic plot of I_{em} versus I_{IR}.[39] As shown in Fig. 13, the slope of the linear fits for the green and red emissions in YOF: Yb^{3+}, Er^{3+}@400 °C sample are 1.05 and 1.82. The dependence of emission intensities on the pumping power density of YOF: Yb^{3+}, Er^{3+}@500 °C sample is identical to that of YOF: Yb^{3+}, Er^{3+}@500 °C. Fig. 14 presents the dependence logarithmic plot of YOF: Yb^{3+}, Er^{3+}@600 °C, and the slope of the linear fits is 1.25 for red emission and 1.88 for green emission, respectively. The slopes of the green emissions are close to 2 , however, the slopes for the red ones are obvious less than 2. In fact, the structure of the calcinated samples is of a porous nature, which could be found by the SEM and TEM images. Meanwhile, the crystal structure fitting and element analysis reveal that there are lattice defects in these samples. The structure and lattice defects might absorb the red light emitted by active centres; this will cause quenching of the red emission and decreasing of the slope of the log (I_{em}) verse log (I_{IR}) plot that corresponding to red emission. Considering that the measured slopes of the red emissions are less than actual ones, one can deduce that the up-conversion emission of per visible photon in rhombohedral YOF: Yb^{3+}, Er^{3+} samples involves absorption of two 980 nm photons. The up-conversion emission mechanism of Er^{3+} ion in rhombohedral YOF: Yb^{3+}, Er^{3+} samples could be explained by the energy levels diagrammatic sketch shown in Fig. 15, which involves three typical energy transfer procedures between Yb^{3+} and Er^{3+} ions (denoted as 1, 2 and 3 in the figure).

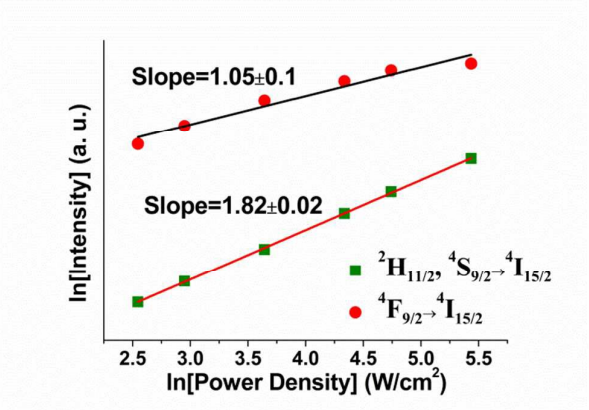

Fig. 13 The dependence of the red and green emission intensities of YOF:Yb^{3+}, Er^{3+}@400 °C sample on pumping power of 980 nm laser excitation.

RSC Advances Accepted Manuscript

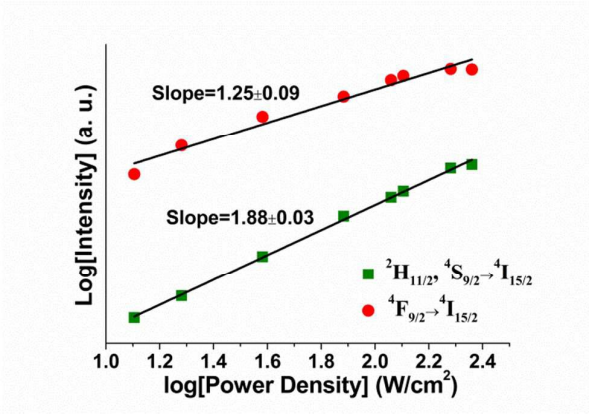

Fig. 14 The dependence of the red and green emission intensities of YOF:Yb^{3+}, Er^{3+}@600 °C sample on pumping power of 980 nm laser excitation.

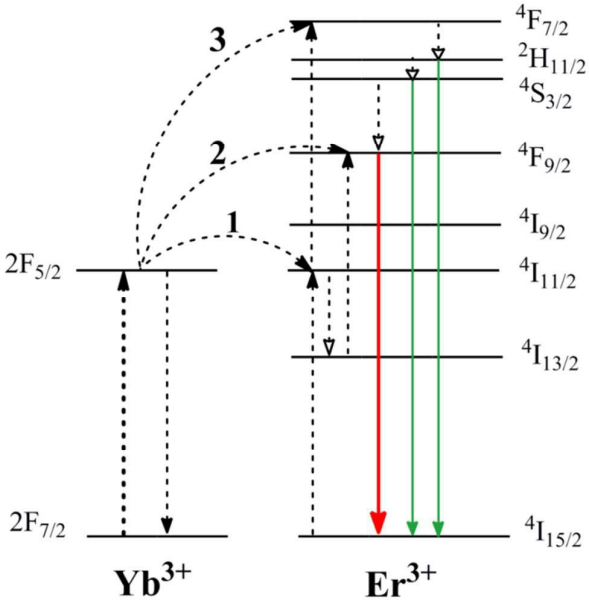

Fig. 15 Energy levels and energy transfer sketch between $Yb^{3+}$and Er^{3+} ions. The dotted lines with upward solid arrow denote absorption transitions; the solid lines with downward solid arrow denote emission transitions; the dotted lines with downward hollow arrow denote phonon assisted non-radiative transitions.

When pumped by 980 nm laser, the Yb^{3+} and Er^{3+} ions are first excited from ground state to $^2F_{5/2}$ (Yb^{3+}) and $^4I_{11/2}$ (Er^{3+}) levels. With the help of energy transfer from Yb^{3+} ion to Er^{+3} ions, different excited energy levels such as $^2H_{11/2}$, $^4S_{3/2}$ and $^4F_{9/2}$ of Er^{3+} ion will be populated. The Yb^{3+} ion would transfer its energy to Er^{3+} ion by $^2F_{5/2}\rightarrow{}^2F_{7/2}$ (Yb^{3+}) : $^4I_{15/2}\rightarrow{}^4I_{11/2}$ (Er^{3+}) process to make the Er^{3+} populate $^4I_{11/2}$ level, this is the energy transfer procedure 1 presented in Fig. 15. When excited to $^4I_{11/2}$ level, Er^{3+} ion will relax to the long lifetime lower lying level $^4I_{13/2}$ by multiphonon emitting procedure. Then, the Yb^{3+} ion would transfer its energy again by process $^2F_{5/2}\rightarrow{}^2F_{7/2}$ (Yb^{3+}) : $^4I_{13/2}\rightarrow{}^4F_{9/2}$ (Er^{3+}) to make the $^4F_{9/2}$ (Er^{3+}) populated. Er^{3+} ions which excited at $^4F_{9/2}$ level will relax to the lowest state $^4I_{15/2}$ by radiative transition and the red emission happens. The energy transfer process involved in this procedure is denoted as 2 in Fig. 15. At the same time, Yb^{3+} could transfer its energy to Er^{3+} ion that populated $^4I_{11/2}$ level to make the $^4F_{7/2}$ level of Er^{3+} ion populated through $^2F_{5/2}\rightarrow{}^2F_{7/2}$ (Yb^{3+}) : $^4I_{11/2}\rightarrow{}^4F_{7/2}$ (Er^{3+}) process. Then Er^{3+} ions reach the green emitting levels $^2H_{11/2}$ and $^4S_{3/2}$ by multiphonon relaxation. The energy transfer process in this procedure is denoted as 3 in Fig. 15.[31,40] It can be seen that both of the red and green emissions of Er^{3+} are relevant to a two photons absorption process.

It is interesting that the UCL spectra of YOF:Yb^{3+}, Er^{3+}@400 °C, 500 °C and 600 °C samples are characteristic of large value of R/G ratio (ratio of red emission intensity to green emission intensity) since all the patterns are dominated by red emission band. Based on the UCL mechanism of Yb^{3+}-Er^{3+} system discussed above, it could be deduced that the population density of Er^{3+} red emitting levels ($^2H_{11/2}$ and $^4S_{3/2}$) is larger than that of Er^{3+} green emitting level $^4F_{9/2}$. Spectroscopy studies of Yb^{3+} and Er^{3+} co-doped up-conversion materials demonstrate that the R/G ratio is influenced by various factors such as morphology and size of particles, doping concentration of Yb^{3+} ion, host materials, surface defect and so on.[41,42] Recently, YOF:Yb^{3+}, Er^{3+} with various morphologies and sizes have been prepared through different method, e.g. YOF:Yb^{3+}, Er^{3+} nano fiber, nanoparticles, spherical hollow particles, micro-rods and micro-box and so on.[15,31,32,43,44] All of the UCL spectra of the reported samples are dominated by red emission band. Meanwhile, M. Y. Ding et.al investigated the influence of Yb^{3+} concentration on the R/G ratio of YOF:Yb^{3+}, Er^{3+} micro-box by tuning the Yb^{3+} concentration from 10 at.% to 30 at.% ($Yb^{3+}/(Y^{3+}+Yb^{3+}+Er^{3+})$).[43] The result reveals that increasing of Yb^{3+} doping level will suppress the population of $^2H_{11/2}$ and $^4S_{3/2}$ levels of Er^{3+} ion by way of back energy transfer, resulting in the decrease of green ($^2H_{11/2}$,$^4S_{3/2}\rightarrow{}^4I_{15/2}$) emission. However, the red emission intensity in the UCL spectrum of YOF:Yb^{3+}, Er^{3+} is still surpass the green emission one obviously even when the Yb^{3+} doping concentration was kept at lower level (10 at.%). It might be the nature of YOF host lattice that favor the red emission for co-doped $Yb^{3+}$and Er^{3+} electronic system.

Conclusions

YOF: Yb^{3+}, Er^{3+} powder has been successfully prepared through a modified Sol-Gel method by using $Re(NO)_3$ and TFA as raw materials and followed by a moderate calcinating procedure. Phase analysis performed based on the XRD data of the products showed that YOF: Yb^{3+}, Er^{3+} powders with rhombohedral symmetry were obtained at the temperature range of 400-600 °C. The relative wider range of calcinating temperature makes this method very feasible to synthesize rhombohedral YOF: Yb^{3+}, Er^{3+} powder. Elements analysis reveals that there are F defects in the lattice of the rhombohedral YOF: Yb^{3+}, Er^{3+} powders. Meanwhile, the distribution of dopant ions is inhomogeneous because the

RSC Advances Accepted Manuscript

This journal is © The Royal Society of Chemistry 20xx

segregation coefficients of Yb^{3+} and Er^{3+} ions are both less than 1. It is observed that the temperature plays a determining role on modulating of the growth phase and evolution of morphology of the Sol-Gel products. The prepared YOF: Yb^{3+}, Er^{3+} powder exhibit efficient red UCL under excitation of 980nm laser irradiation. The product obtained through this method exhibits good repetitiveness and is promising candidate in red emitting luminescent materials.

Acknowledgements

This work was financially supported by the National Natural Science Foundation of China (Grant Nos 61308085, 51102047, 51472050 and 11404072).

Notes and references

1 M. Shang, D. Geng, X. Kang, D. Yang, Y. Zhang and J. Lin, *Inorg. Chem.*, 2012, **51**, 11106.
2 G. Yi, Y. Peng and Z. Gao, *Chem. Mater.*, 2011, **23**, 2729-2734.
3 Y. Zhang, D. Geng, X. Kang, M. Shang, Y. Wu, X. Li, H. Lian, Z. Cheng and J. Lin, *Inorg. Chem.*, 2013, **52**, 12986.
4 X. Huang, S. Han, W. Huang and X. Liu, *Chem. Soc. Rev.*, 2013, **42**, 173.
5 R. Naccache, Q. Yu and J. A. Capobianco, *Adv. Opt. Mater.*, 2015, **3**, 482.
6 W. Shao, G. Chen, T. Y. Ohulchanskyy, A. Kuzmin, J. Damasco, H. Qiu, C. Yang, H. Agren and P. N. Prasad, *Adv. Opt. Mater.*, 2015, **3**, 575.
7 S. Zhao, F. Zheng, S. Xu, H. Wang and B. Wang, *Chin. Opt. Lett.*, 2009, **7**, 416.
8 J. Hölsä, B. Piriou and M. Räsänen, *Spectrochim. Acta a*, 1993, **49**, 465.
9 N. Rakov, R. B. Guimarães, W. Lozano B. and G. S. Maciel, *J. Appl. Phys.*, 2013, **114**, 43517.
10 B. Shao, Q. Zhao, W. Lv, M. Jiao, W. Lue and H. You, *Adv. Opt. Mater.*, 2015, **3**, 583.
11 J. Wang, J. Lin, J. Wu, M. Huang, Z. Lan, Y. Chen, S. Tang, L. Fan and Y. Huang, *Electrochim. Acta*, 2012, **70**, 131.
12 S. E. Dutton, D. Hirai and R. J. Cava, *Mater. Res. Bull.*, 2012, **47**, 714.
13 N. Rakov and G. S. Maciel, *Opt. Mater.*, 2013, **35**, 2372.
14 N. Rakov, J. D. A. B. Barbosa, R. B. Guimaraes and G. S. Maciel, *J. Alloy. Compd.*, 2012, **534**, 32.
15 N. Rakov, S. A. Vieira, R. B. Guimaraes and G. S. Maciel, *J. Alloy. Compd.*, 2015, **618**, 127.
16 Y. Tian, B. Chen, R. Hua, J. Sun, L. Cheng, H. Zhong, X. Li, J. Zhang, Q. Meng and M. Chen, *J. Nanosci. Nanotechno.*, 2011, **11**, 9631.
17 T. Wen, W. Luo, Y. Wang, M. Zhang, Y. Guo, J. Yuan, J. Ju, Y. Wang, F. Liao and B. Yang, *J. Mater. Chem. C*, 2013, **10**, 1995.
18 R. Li, L. Li, W. Zi, J. Zhang, L. Liu, L. Zou and S. Gan, *New J. Chem.*, 2015, **39**, 115.
19 R. Yang, G. Qin, D. Zhao, K. Zheng and W. Qin, *J. Fluorine Chem.*, 2012, **140**, 38.
20 T. Grzyb and S. Lis, *Inorg. Chem.*, 2011, **50**, 8112-8120.
21 T. Grzyb, M. Węcławiak and S. Lis, *J. Alloy. Compd.*, 2012, **539**, 82.
22 T. Grzyb, M. Węcławiak, J. Rozowska and S. Lis, *J. Alloy. Compd.*, 2013, **576**, 345.
23 D. J. M. Bevan, J. Mohyla, B. F. Hoskins and R. J. Steen, Eur. *J. Solid State Inorg. Chem.*, 1990, **27**, 451.
24 L. Y. Li, Y. Yu, G. F. Wang, L. Z. Zhang and Z. B. Lin, *CrystEngComm*, 2013, **15**, 6083.
25 X. Y. Huang, Z. B. Lin, L. Z. Zhang and G. F. Wang, *J. Cryst. Growth*, 2007, **306**, 208
26 R. A. Laudise, E. D. Kolb and A. J. Caporaso, *J. Am. Ceram. Soc.*, 1964, **47**, 9.
27 S. Mann, *Angew. Chem. Int. Edit.*, 2000, **39**, 3393-3406.
28 I. Levin, Q. Z. Huang, L. P. Cook and W. Wong-Ng, *Eur. J. Inorg. Chem.*, 2005, **36**, 87.
29 J. Hölsä and E. Kestilä, *J. Alloy. Compd.*, 1995, **225**, 89-94.
30 J. Hölsä and E. Kestilä, *J. Chem. Soc., Faraday Trans.*, 1995, **91**, 1503.
31 T. Passuello, F. Piccinelli, M. Pedroni, S. Polizzi, F. Mangiarini, F. Vetrone, M. Bettinelli and A. Speghini. *Opt. Mater.* 2011, **33**, 1500.
32 Y. Zhang, X. J. Li, D. L. Geng, M. M. Shang, H. Z. Lian, Z. Y. Cheng and J. Lin, *CrystEngComm*, 2014, **16**, 2196.
33 L. Liu, E. Ma, R. Li, G. Liu and X. Chen, *Nanotechnology*, 2007, **18**, 488.
34 Q. Xiao, Y. Liu, L. Liu, R. Li, W. Luo and X. Chen, *J. Phys. Chem. C*, 2010, **114**, 9314.
35 Y. Liu, W. Luo, R. Li, G. Liu, M. R. Antonio and X. Chen, *J. Phys. Chem. C*, 2008, **112**, 686.
36 W. Zheng, D. Tu, P. Huang, S. Zhou, Z. Chen and X. Chen, *Chem. Commun.*, 2015, **51**, 4129.
37 J. C. Boyer, F. Vetrone, J. A. Capobianco, A. Speghini and M. Bettinelli, *J. Phys. Chem. B*, 2004, **108**, 20137.
38 L. Y. Li, Y. Yu, G. F. Wang and L. Z. Zhang, *RSC Adv.*, 2014, **4**, 37041.
39 N. Niu, P. Yang, F. He, X. Zhang, S. Gai, C. Li and J. Lin, *J. Mater. Chem.* 2012, **22,** 10889.
40 M. Haase and H. Schäfer. *Angew. Chem. Int. Ed.* 2011, **50**, 5808.
41 H. X. Mai, Y. W. Zhang, L. D.Sun and C. H. Yan, *J. Phys. Chem. C* 2007**, 111***,* 13721.
42 S. Schietinger, L. de S. Menezes, B. Lauritzen, and O. Benson, *Nano Lett.*, 2009, **9**, 2477.
43 M. Y. Ding, C. H. Lu, L. H. Cao, Y. R. Ni and Z. Z. Xu, *Opt. Mater.* 2013, **35,** 1283.
44 E. Martinez-Castro, J. García-Sevillano, F. Cussó and M. Ocaña, *J. Alloys Compd.,* 2015, **619,** 44.

RSC Advances Accepted Manuscript

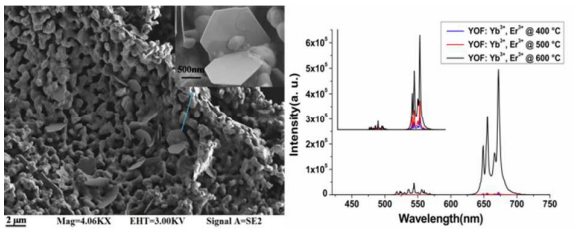

Rhombohedral YOF: Yb^{3+}, Er^{3+} prepared by calcinating exhibit duality of morphology; Efficient red light emission could be obtained when the powders are excited by 980 nm laser beam.

RSC Advances Accepted Manuscript